JOURNAL OF PROPULSION AND POWER
Vol. 16, No. 3, May–June 2000

Flow of Gel Fuels in Tapered Injectors

Shai Rahimi* and Benveniste Natan†
Technion—Israel Institute of Technology, 32000 Haifa, Israel

The governing equations of the steady flow of gel propellants and fuels in a tapered tube injector have been formulated assuming a power-law rheological model. A parametric investigation was conducted to evaluate the effect of the injector geometry and pressure gradient on the flow rate and the mean apparent viscosity of the gel for various fuels and metal loadings. The theoretical results indicate that the flow rate increases significantly with decreasing the power-law index and with increasing the pressure drop in the injector. The apparent viscosity is not uniform in each cross section; it is maximal at the axis and reaches minimum at the wall. The mean apparent viscosity of the gel exhibits a significant decrease with increasing the convergence angle of the injector. This implies that to obtain better atomization of the gel, high convergence angles are required. A comparison between RP-1/Al gels with various aluminum mass fractions was conducted. The results indicate the existence of an optimal metal loading.

Nomenclature

D	= diameter
$I_{1,2,3}$	= invariants
k	= viscous constant
L	= length of pipe
n	= power-law index
P	= pressure
R_Z	= radius
r, θ, z	= cylindrical coordinates
r^*	= normalized radius, equal to r/R_z
T	= temperature
t	= time
u	= fluid velocity
$\dot{V}$	= volumetric flow rate
z^*	= normalized axial position, equal to z/L
α	= wall inclination angle
$\dot{\gamma}$	= shear rate
$\underset{\approx}{\dot{\gamma}}$	= rate-of-strain tensor
$\underset{\approx}{\eta}$	= non-Newtonian viscosity
$\bar{\eta}$	= mean apparent viscosity
λ	= decay structural parameter
μ	= Newtonian viscosity
ρ	= propellant density
$\underset{\approx}{\tau}$	= stress tensor deviator
$\underset{\approx}{\tau}_0$	= yield stress

Subscripts

e	= equilibrium value
i, j, k	= indices
L	= injector exit plane
w	= wall
0	= injector inlet plane

Introduction

GEL propellants are fuels and oxidizers whose rheological properties have been altered by the addition of gelling agents and metal loading additives, such that they behave as time-dependent non-Newtonian viscoelastic fluids. These propellants are advantageous because of either their safety and performance benefits.

Gel propellants provide safety over conventional liquids and solid propellants and have been shown to meet most of the insensitive munitions and minimum smoke criteria without performance losses.[1] Their performance characteristics and operational capabilities, which are similar to liquid propellants, as well as their high density, increased combustion energy, and long-term storage capability, make them attractive for many applications,[2,3] especially for volume-limited propulsion systems.[4–6]

The addition of gelling agents can prevent agglomeration, aggregation, and separation of the metal solid phase from the fuel during storage by constructing a three-dimensional matrix by the intermixing of their long polymeric chains. However, these gelling agents can also cause the gel viscosity to increase, which makes the fuel more difficult to atomize and reach high combustion efficiency in the rocket engines.[3–5]

One of the most important characteristics of gel propellants and fuels is that their viscosity is shear-rate dependent (non-Newtonian). Considering this rheological behavior of the gel propellants, by applying high shear rates during injection it is possible to reach low viscosities and even liquidification near the injector exit.[5,7] The decrease in viscosity with increasing shear rate is referred to as shear thinning, and the fluid is defined as shear thinning or pseudoplastic. This effect can be quite dramatic, with the viscosity decreasing by a factor[8,9] of as much as 10^3 or 10^4.

The viscosity of gels is significantly affected by the temperature and by the mass fraction of metals in the gel mixture. Gupta et al.[10] measured the power and viscosity indices, n and k, respectively, of UDMH-MC with aluminum and magnesium at various compositions and temperatures. However, their results are presented such that they cannot be used. Though power index n is valid, the presented viscosity index k is calculated on the basis of the Haake viscometer dial reading (proportional to the shear stress) and the viscometer revolutions per minute (proportional to the shear rate). The real viscosity index has to be calculated from the actual shear stress and rate (which are of course known to the authors of Ref. 10 but not reported). The result is that the real k is not just proportional to the presented k, but also depends on the power index by an unknown relation. This fact reduces significantly the value of the reported experimental results not only quantitatively but also qualitatively. Rapp and Zurawski[5] conducted a very thorough experimental investigation on the rheological properties of RP-1/Al gel fuels. According to their findings, these fuels exhibit shear thinning behavior; however, they are unstable for aluminum mass fractions below 45%. In general, for the same shear stress the viscosity decreased with decreasing the metal loading (also indicated by Gupta et al.[10] for UDMH propellants). The experimental results are mainly qualitative, as also claimed by the authors.[5]

Received 30 January 1996; revision received 20 January 1999; accepted for publication 21 January 1999.

*Graduate Student, Faculty of Aerospace Engineering.
†Senior Lecturer, Faculty of Aerospace Engineering. Senior Member AIAA.

To approximate the rheological behavior of gel propellant polymeric systems power-law (PL) rheological constitutive equations (RCE) have been proposed in many studies.[3,7,10,11] The PL (or Ostwald–deWaele) model is an empirical relationship[12] that describes the shear-stress tensor as a function of the rate-of-strain tensor. With the appropriate choice of material constants or functions, these equations describe satisfactorily the experimental data for some types of flows. However, experience shows that, under certain conditions, the theoretical results are in significant quantitative, even qualitative, disagreement with experiments.[9] The region of non-Newtonian flow behavior in which viscosity varies strongly with shear stress and rate is limited by extreme values of viscosities that are independent of the shear rate and stress.[13] Injection of the gel propellant through a tapered injector causes the shear rate to increase and, consequently, results in a decrease in viscosity along the axis of the injector.

The problem of laminar flow in cylindrical tubes was studied by Bird et al.[8] Analytical solutions for steady flow of PL fluids in cylindrical tubes with constant cross section were presented by Skelland,[14] Kozicki and Tiu,[15] and Cheremisinoff.[16] Ta-Jo[17] and Karagiannis et al.[18] determined the pressure drop–flow rate relationship for PL fluids by the Galerkin finite element method, which is applicable to ducts of any geometry.

The theory of the steady slow motion of a non-Newtonian fluid through a slightly tapered tube was purposed by Syoten and Tadayoshi.[19] General analytical formulas for the shear stress, velocity, and pressure gradient based on the assumption that the semi-angle of the cone is small also were presented by Sutterby,[20] Syoten,[21] and Papanastasiou.[22] Dijksman and Savenije[23] used a special toroidal coordinate system to analyze the flow of non-Newtonian liquids through pipes.

Though the flow of non-Newtonian fluids has been thoroughly studied, there are only a few papers published in the open literature that deal with the injection process of gel propellants and fuels. The atomization of metallized gel slurry fuels for ramjet applications has been studied by Netzer's group (see Ref. 4) at the Naval Postgraduate School using commercial atomizers. Green et al.[3] provided a flow visualization of gel simulants using triplet and coaxial injectors. The apparent viscosity of the fluid at the exit of the injector was calculated for a constant strain rate. Chojnacki and Feikema[24] investigated the atomization of water gels using a like-on-like doublet injector. In this work,[24] the fluid injection system was transformed to a capillary viscometer to measure the viscosity of the non-Newtonian gel. However, in all studies, the atomizers used were standard and not designed for non-Newtonian flow. A more detailed analysis of the flow of gel propellants and fuels for various injector geometries can be a rather useful tool for the prediction of the apparent viscosity and, consequently, for the atomization.

The formulation of the governing equations for the unsteady, incompressible, isothermal, and laminar non-Newtonian gel propellant flow through a tapered tube by using the PL model for the gel propellant RCEs is one aspect of the present work. For further analysis of the flow behavior of several gel fuels, a steady motion and a small semi-angle of the cone is assumed. A parametric investigation was conducted to evaluate the effect of the injector geometry and pressure gradient on the flow rate and the mean apparent viscosity of the gel at the injector exit plane, for various fuel types and metal loadings.

The values of the rheological properties of the gels used in the present study were measured experimentally and also taken from literature.

Theoretical Model

Rheological Constitutive Equations

A rheological equation relates stress or deformation to flow variables of materials such as strain, shear rate, and time. The time-independent PL empirical model[3,7,10,11] describes satisfactorily the rheological behavior of gel propellants. The equation is expressed by[12]

$$\underset{\approx}{\tau} = \eta \underset{\approx}{\dot{\gamma}} \tag{1}$$

where η is the non-Newtonian viscosity (apparent viscosity) defined by

$$\eta = k|\dot{\gamma}|^{n-1} \tag{2}$$

Because the non-Newtonian viscocity, which is a scalar, depends on the rate-of-strain tensor, it must depend only on those particular combinations of components of the tensor that are independent of the coordinate system.[8] Three independent combinations may be selected,

$$I_1 = \sum_i \dot{\gamma}_{ij} \tag{3}$$

$$I_2 = \sum_i \sum_j \dot{\gamma}_{ij}\dot{\gamma}_{ji} \tag{4}$$

$$I_3 = \sum_i \sum_j \sum_k \dot{\gamma}_{ij}\dot{\gamma}_{jk}\dot{\gamma}_{ki} \tag{5}$$

For an incompressible fluid $I_1 = 2(\nabla \cdot \boldsymbol{u}) = 0$. The value of invariant I_3 vanishes for shearing flows in simple geometries such as an axisymmetric tube.[8,20] Hence, η is taken to be dependent on the shear rate $\dot{\gamma}$, which is a function of invariant I_2 only, and is given by

$$\dot{\gamma} = \sqrt{\frac{1}{2}\sum_i \sum_j \dot{\gamma}_{ij}\dot{\gamma}_{ji}} = \sqrt{\frac{1}{2}\left(\underset{\approx}{\dot{\gamma}} : \underset{\approx}{\dot{\gamma}}\right)} \tag{6}$$

The PL RCE is given by

$$\underset{\approx}{\tau} = -k\left[\tfrac{1}{2}\left(\underset{\approx}{\dot{\gamma}} : \underset{\approx}{\dot{\gamma}}\right)\right]^{(n-1)/2} \underset{\approx}{\dot{\gamma}} \tag{7}$$

For $0 < n < 1$, the fluid is pseudoplastic (possessing shear thinning), whereas for $n > 1$, it is dilatant (possessing shear thickening). In the case of $n = 1$, Eq. (7) describes a Newtonian viscous fluid with constant viscosity $k = \mu$. Shear thinning fluids, described by a PL model lead to increasingly nonlinear equations as n is decreased.[18]

Assumptions

For the flow analysis the following assumptions are made.

1) The flow is incompressible, laminar, and isothermal with axial symmetry, and no body forces act on the fluid.

2) The gel propellant RCE obeys the PL model.

3) All losses in the injector are ignored.

In a later stage two additional assumptions are made to simplify the problem and to analyze the flow behavior of several gel fuels.

4) The motion is steady.

5) The semi-angle of the cone is small.

Flow Geometry and Boundary Conditions

The geometries shown in Fig. 1 are considered: Fig. 1a converging tube and Fig. 1b tube with constant cross section. The coordinate system is defined along the r, θ, and z axes. The radius changes gradually from R_0 to R_L over the distance L. The wall-line equation is given by

$$R_Z = R_0 + \frac{R_L - R_0}{L} \cdot z \tag{8}$$

The overall pressure drop is $(P_0 - P_L) \equiv \Delta P$.

Governing Equations

On the basis of the assumptions 1–3, the equations of continuity and momentum conservation become

$$\frac{\partial \rho}{\partial t} + \nabla \cdot (\rho \boldsymbol{u}) = 0 \tag{9}$$

$$\rho\left(\frac{\partial \boldsymbol{u}}{\partial t} + (\boldsymbol{u} \cdot \nabla)\boldsymbol{u}\right) = -\nabla \cdot \underset{\approx}{\tau} - \nabla P \tag{10}$$

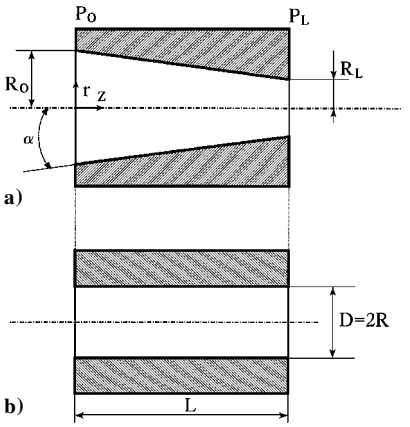

Fig. 1 Injector geometry: a) tapered and b) constant cross section area.

The rate-of-strain tensor is given by

$$\underset{\approx}{\dot{\gamma}} = \nabla \cdot \boldsymbol{u} + (\nabla \cdot \boldsymbol{u})^T \tag{11}$$

From the axial symmetry of the fluid motion, it can be seen that $u_\theta = 0$, that $\partial/\partial\theta = 0$, and that u_r and u_z are functions of r and z alone. In this case the rate-of-strain tensor reduces to

$$\underset{\approx}{\dot{\gamma}} = \begin{bmatrix} 2\dfrac{\partial u_r}{\partial r} & 0 & \dfrac{\partial u_r}{\partial z} + \dfrac{\partial u_z}{\partial r} \\ 0 & 2\dfrac{u_r}{r} & 0 \\ \dfrac{\partial u_r}{\partial z} + \dfrac{\partial u_z}{\partial r} & 0 & 2\dfrac{\partial u_z}{\partial z} \end{bmatrix} \tag{12}$$

Substituting Eq. (12) into Eq. (7) provides the expressions for the relevant components of the stress tensor $\underset{\approx}{\tau}$

$$\tau_{rr} = -2k\dot{\gamma}^{n-1} \cdot \left(\frac{\partial u_r}{\partial r}\right) \tag{13}$$

$$\tau_{rz} = \tau_{zr} = -k\dot{\gamma}^{n-1} \cdot \left(\frac{\partial u_r}{\partial z} + \frac{\partial u_z}{\partial r}\right) \tag{14}$$

$$\tau_{zz} = -2k\dot{\gamma}^{n-1}\left(\frac{\partial u_z}{\partial z}\right) \tag{15}$$

Substituting Eq. (12) into Eq. (6) provides the expression for the shear rate $\dot{\gamma}$

$$\dot{\gamma} = \sqrt{2\left[\left(\frac{\partial u_r}{\partial r}\right)^2 + \left(\frac{u_r}{r}\right)^2 + \left(\frac{\partial u_z}{\partial z}\right)^2\right] + \left[\frac{\partial u_r}{\partial z} + \frac{\partial u_z}{\partial r}\right]^2} \tag{16}$$

Under the assumption of steady-state motion, all $\partial/\partial t$ become zero. Assuming a small cone semi-angle u_r, $\partial u_r/\partial z$ and $\partial u_r/\partial r$ also become zero. To satisfy continuity, $\partial u_z/\partial z = 0$, too. If the flow accelerates, the axial velocity gradient with z is not zero; however, it is of the order of magnitude of $\mathcal{O}(\alpha)$ compared to the gradient of u_z in the radial direction [$\sim\mathcal{O}(1)$]. Thus, the equation of momentum conservation described by Eq. (10) is reduced to a single equation for the axial direction,

$$-\frac{\mathrm{d}P}{\mathrm{d}z} + \frac{1}{r}\frac{\partial}{\partial r}(r\tau_{rz}) = 0 \tag{17}$$

In this case, Eq. (14) becomes $\tau_{rz} = -k\dot{\gamma}^{n-1} \cdot (\partial u_z/\partial r)$. Substitution of Eq. (14) into Eq. (17) and integration within a cross section, considering that the velocity gradient is zero at the axis, yields

$$-k\left(-\frac{\partial u_z}{\partial r}\right)^n = \frac{r}{2}\frac{\mathrm{d}P}{\mathrm{d}z} \tag{18}$$

Second integration within a cross section, considering no-slip conditions at the wall ($r = R_Z$, $u_z = 0$), gives

$$u_z = \frac{n}{n+1} \cdot \left(-\frac{1}{2k}\frac{\mathrm{d}P}{\mathrm{d}z}\right)^{1/n} \cdot R_Z^{(n+1)/n} \cdot \left[1 - \left(\frac{r}{R_Z}\right)^{(n+1)/n}\right] \tag{19}$$

The volumetric flow rate is defined as

$$\dot{V} = 2\pi \int_0^{R(z)} r u_z \,\mathrm{d}r \tag{20}$$

Substitution of Eq. (19) into Eq. (20) and integration yields

$$\dot{V} = \frac{n}{3n+1} \cdot \pi \cdot \left[\left(-\frac{1}{2k}\right)\left(\frac{\mathrm{d}P}{\mathrm{d}z}\right)\right]^{1/n} \cdot R_Z^{(3n+1)/n} \tag{21}$$

Assuming that the volumetric flow rate is constant due to the incompressibility of the fluid, the pressure profile can be determined from Eq. (21),

$$P(z) = P_0 - \frac{2k \cdot L}{3n \cdot (R_0 - R_L)} \cdot \left[\frac{\dot{V}(3n+1)}{\pi \cdot n}\right]^n \cdot \left(R_Z^{-3n} - R_0^{-3n}\right) \tag{22}$$

Substituting the boundary condition $P(z = L) = P_L$ into Eq. (22), the volumetric flow rate is described by

$$\dot{V} = \frac{\pi \cdot n}{(3n+1)} \cdot \left[\frac{3n \cdot (P_0 - P_L) \cdot (R_0 - R_L)}{2k \cdot L \cdot \left(R_L^{-3n} - R_0^{-3n}\right)}\right]^{1/n} \tag{23}$$

Pressure Distribution

Substitution of Eq. (23) into Eq. (22) yields the pressure profile under fixed inlet and outlet pressures P_0 and P_L as follows:

$$P(z) = P_0 - (P_0 - P_L) \cdot \frac{R_Z^{-3n} - R_0^{-3n}}{R_L^{-3n} - R_0^{-3n}} \tag{24}$$

The pressure decreases with increasing z, linearly for $\alpha = 0$ and parabolically for $\alpha > 0$ and $0 < n \leq 1$.

Velocity Distribution

Expressing $\mathrm{d}P/\mathrm{d}z$ from Eq. (24) and substituting it into Eq. (19) yields

$$u_z = \left[\frac{3n \cdot (P_0 - P_L) \cdot (R_0 - R_L)}{2k \cdot L \cdot \left(R_L^{-3n} - R_0^{-3n}\right)}\right]^{1/n} \times \frac{n}{n+1} \cdot \frac{1}{R_Z^2} \cdot \left[1 - \left(\frac{r}{R_Z}\right)^{(n+1)/n}\right] \tag{25}$$

The velocity gradients $\partial u_z/\partial r$ and $\partial u_z/\partial z$ are, respectively, given by

$$\frac{\partial u_z}{\partial r} = -\left[\frac{3n \cdot (P_0 - P_L) \cdot (R_0 - R_L)}{2k \cdot L \cdot \left(R_L^{-3n} - R_0^{-3n}\right)}\right]^{1/n} \cdot \frac{1}{R_Z^3} \cdot \left(\frac{r}{R_Z}\right)^{1/n} \tag{26}$$

$$\frac{\partial u_z}{\partial z} = \left[\frac{3n \cdot (P_0 - P_L) \cdot (R_0 - R_L)}{2k \cdot L \cdot \left(R_L^{-3n} - R_0^{-3n}\right)}\right]^{1/n} \cdot \frac{n}{n+1} \cdot \frac{1}{R_Z^3} \times \left[2 - \frac{3n+1}{n} \cdot \left(\frac{r}{R_Z}\right)^{(n+1)/n}\right] \cdot \frac{R_0 - R_L}{L} \tag{27}$$

It can be clearly seen from Eqs. (26) and (27) that the previous assumption of $(\partial u_z/\partial z)/(\partial u_z/\partial r) = \mathcal{O}(\alpha)$, where $\alpha = (R_0 - R_L)/L$, is quite justified everywhere, except near the axis where $\partial u_z/\partial r$ vanishes.

Definition of the Mean Apparent Viscosity

The apparent viscosity described by Eq. (2) is not uniform in each cross section. This means that the fluid properties vary with radius and that momentum is not transferred equally at the axis and at the wall. To evaluate the effect of the convergence of the injector on the viscosity, the mean apparent viscosity at the injector exit plane is defined as

$$\bar{\eta}_L = 2k \cdot \int_0^1 \left(\frac{r}{R_L}\right) \dot{\gamma}^{n-1}\Big|_{z=L} \, \mathrm{d}\left(\frac{r}{R_L}\right) \tag{28}$$

To consider the effect of the velocity gradient $\partial u_z/\partial z$ near the axis, Eq. (15) is reduced to

$$\dot{\gamma} = \sqrt{2\left(\frac{\partial u_z}{\partial z}\right)^2 + \left(\frac{\partial u_z}{\partial r}\right)^2} \tag{29}$$

Substituting Eq. (29) into Eq. (28) yields

$$\bar{\eta}_L = 2k \cdot \int_0^1 \left(\frac{r}{R_L}\right) \cdot \left[2\left(\frac{\partial u_z}{\partial z}\right)^2_{z=L} + \left(\frac{\partial u_z}{\partial r}\right)^2_{z=L}\right]^{(n-1)/2} \mathrm{d}\left(\frac{r}{R_L}\right) \tag{30}$$

Substitution of Eqs. (26) and (27) into Eq. (30) and simple numerical integration provide the value of the mean apparent viscosity $\bar{\eta}_L$.

Evaluation of the Rheological Properties

As mentioned in the Introduction, an effort was made to evaluate the effect of the injector geometry and pressure gradient on the flow rate and the mean apparent viscosity of the gel at the injector exit plane, for various fuel types and metal loadings. To demonstrate these effects, the rheological properties of various gels were measured experimentally and also taken from the literature.[3,5] Reference 3 provides the PL for water gel and for RP-1/Al gel. It is mentioned that the RP-1/Al gel contained 55% aluminum with no reference to the aluminum particle sizes in the mixture. Reference 5 provides experimental results for the viscosity of RP-1/Al gels with 5- and 16-μm aluminum particles measured by a Haake viscometer. The data is limited to viscosity measurements at three strain rates at the low strain rate range. Insufficient information was provided for the 5-μm particles, thus no PL can be reduced. As regards the 16-μm particles, the PLs that can be extracted describe the behavior of the gel viscosity qualitatively rather than quantitatively. In any case, the accuracy of the experimental results of Refs. 3 and 5 is not reported. The power and viscosity indices from Refs. 3 and 5 are shown in Table 1.

Table 1 PL data of various gels

Gel type	k, mPa · s^n	n
Water gel[a]	16,750	0.4056
RP-1/Al gel[a]	13,480	0.4728
RP-1/Al 45% Al[b]	271.0	0.881
RP-1/Al 50% Al[b]	1,098.7	0.706
RP-1/Al 55% Al[b]	937.9	0.689
RP-1/Al 60% Al[b]	964.3	0.747
Water gel, 0.3% X[c]	13,960	0.3797
Water gel, 0.5% X[c]	22,880	0.3632
Water gel, 0.75% X[c]	30,610	0.3567
Water gel, 1% Z[c]	17,840	0.4468

[a]From Ref. 3.
[b]Calculated from the results of Ref. 5.
[c]Obtained experimentally in present research.

Experimental Characterization of Water Gels

The purpose of the experimental investigation was to characterize the rheological behavior of water gels with various gellants (X and Z). A TA CSL^2_{100} Carri–Med rheometer was employed for the measurement of the rheological constants. The rheological PL indices of the water gels with X and Z are shown in Table 1. The accuracy of the experimental results was ±2%.

Results and Discussion

The geometry of a converging injector was selected for the parametric investigation. The convergence angle α varied from 0 to 8 deg for pressure drops from 1 to 9 bar. The injector length L chosen was 8 mm, and the injector exit radius R_L varied from 0.2 to 0.4 mm.

The velocity profiles for RP-1/Al gel in a 2-deg angle, 0.4-mm exit radius, converging injector for a 2-bar pressure drop are presented in Fig. 2. As expected, the flow accelerates as the gel moves downstream, and higher velocities are obtained.

The pressure drop is shown in Fig. 3a, and it is almost linear for the 2-deg angle. Increasing the convergence angle to 8 deg

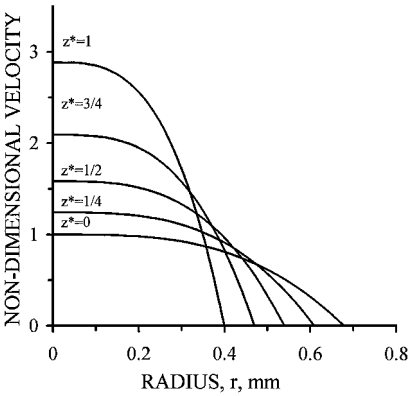

Fig. 2 Velocity profiles for RP-1/Al gel, $z^* = z/L$, $L = 8$ mm, $R_L = 0.4$ mm, $\alpha = 2$ deg, and $\Delta P = 2$ bar.

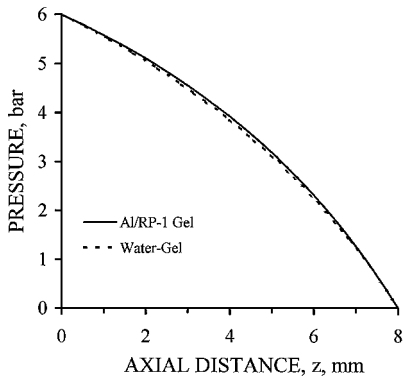

a) $R_L = 0.4$ mm, $\alpha = 2$ deg

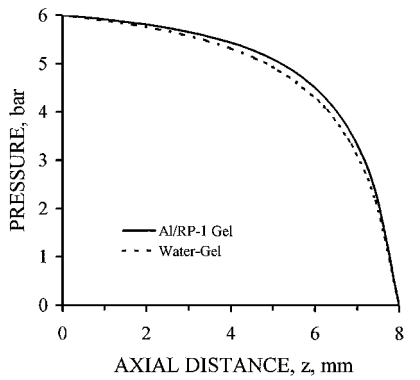

b) $R_L = 0.22$ mm, $\alpha = 8$ deg

Fig. 3 Pressure distribution along the injector axis, for RP-1/Al gel and water gel, $L = 8$ mm.

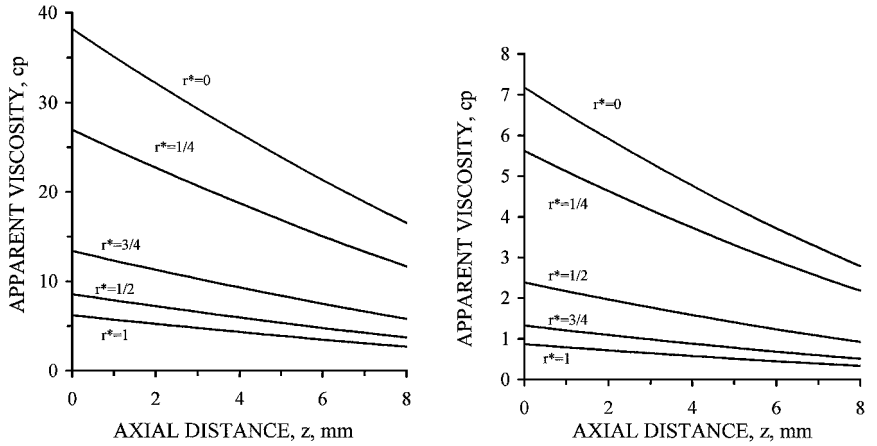

a) RP-1/Al gel b) Water gel

Fig. 4 Apparent viscosity distribution along the axis, $r^* = r/R(z)$, L = 8 mm, R_L = 0.4 mm, α = 2 deg and ΔP = 6 bar.

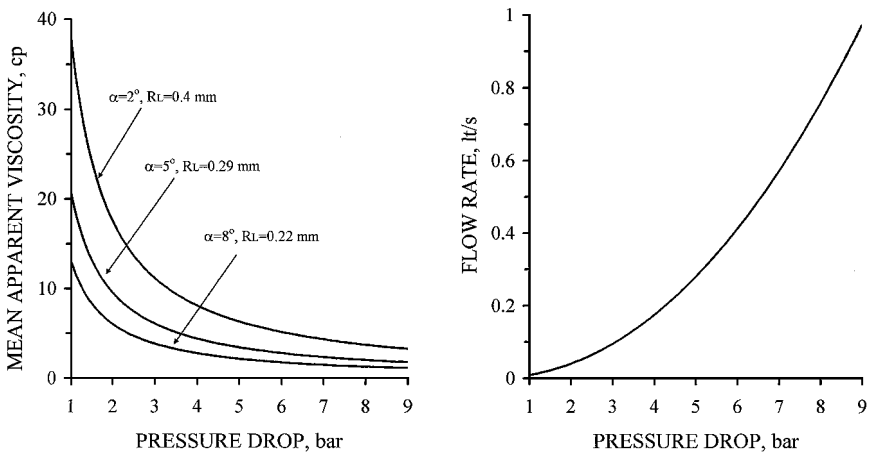

a) Mean apparent viscosity vs pressure drop for various geometries

b) Flow rate (approximate within a 2% range for the preceding geometries) vs pressure drop

Fig. 5 Geometry effect, RP-1/Al gel, L = 8 mm.

results in a more parabolic profile, as shown in Fig. 3b. For both cases it is shown that the pressure gradient is not constant along the axis but increases with decrease in the radius of the tapered tube.

The apparent viscosity distribution for a 6-bar pressure drop is presented in Figs. 4a and 4b for RP-1/Al gel and water gel, respectively. The behavior of the viscosity is the same for both gels; however, the viscosity values for RP-1/Al gel are much larger. The viscosity is maximum at the axis and reaches minimum at the wall. This phenomenon is natural because the velocity gradient $\partial u/\partial r$ is zero at the axis and is maximum at the wall. In general, the viscosity decreases as the gel moves downstream.

The effect of the convergence angle of the injector on the mean apparent viscosity at the injector exit is shown in Fig. 5a for the whole range of the pressure drop. Three angles are presented: 2, 5, and 8 deg. The injector exit diameters were calculated to give approximately the same flow rate for all three angles. The flow rate is shown in Fig. 5b as a function of pressure drop. In general, Eq. (22) indicates that the flow rate increases with decreasing the power index of the PL.

The flow rate also increases with increasing the pressure drop, and the increase is rather sharp for large values of ΔP. However, for pressure drops higher than 5 bar, the decrease of the mean apparent viscosity is small. From Fig. 5a it can be concluded that the mean apparent viscosity can be reduced significantly by increasing the convergence angle. For a pressure drop of 4 bar, the mean apparent viscosity at the exit of a straight injector is reduced by an order of magnitude when an 8-deg convergence-angle injector is used. This is very important and implies that, to obtain better atomization of the gel, high convergence angles are required.

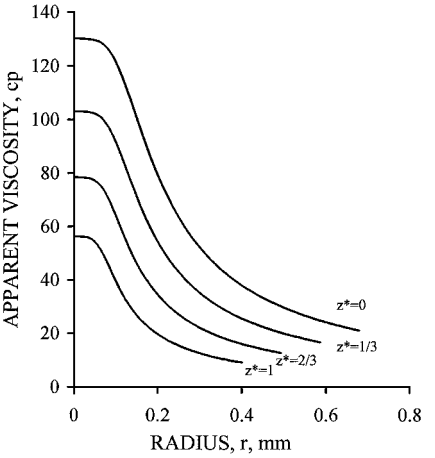

Fig. 6 Apparent viscosity distribution for RP-1/Al gel at various axial locations, L = 8 mm, R_L = 0.4 mm, and α = 2 deg.

The calculation was limited to small convergence angles up to 8 deg. Bigger convergence angles gave unrealistically high flow rates. This is due to the limitation of the analytical solution of the theoretical model and not because of physical reasons.

Figure 6 shows the apparent viscosity distribution at various axial locations of a 2-deg convergence-angle injector for the RP-1/Al gel from Ref. 3. As mentioned earlier, the viscosity reaches its maximum value at the axis and reduces as the gel moves downstream. A comparison between the RP-1/Al gels with various aluminum mass

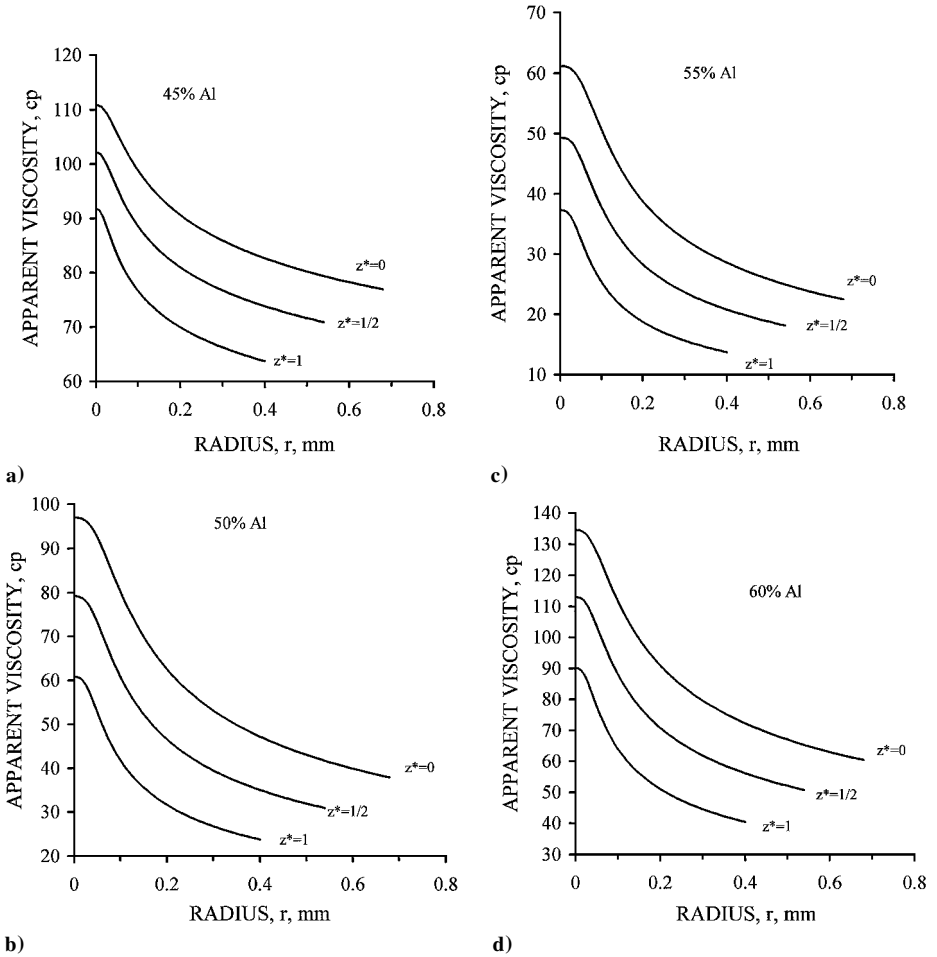

Fig. 7 Apparent viscosity distribution for RP-1/Al gels with various aluminum loadings, at three axial locations, L = 8 mm, R_L = 0.4 mm, and α = 2 deg.

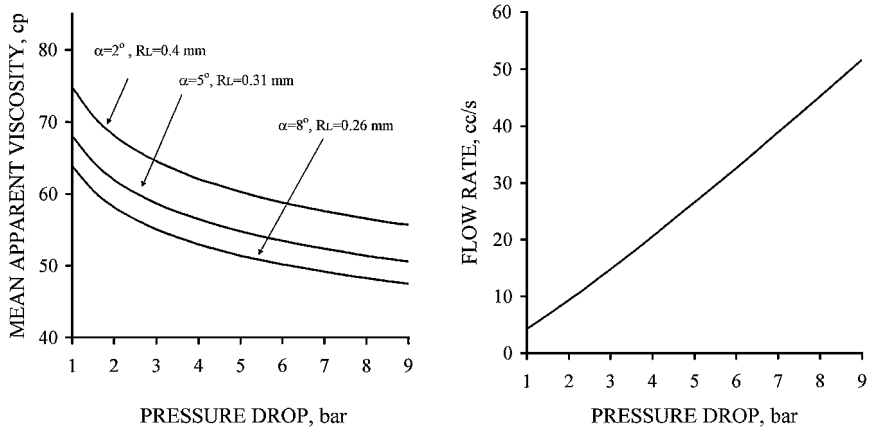

a) Mean apparent viscosity vs pressure drop for various geometries

b) Flow rate (approximate within a 2% range for the preceding geometries) vs pressure drop

Fig. 8 Geometry effect, RP-1/Al gel 45% Al, L = 8 mm.

fractions is shown in Figs. 7a–7d. Each gel (45, 50, 55, and 60% aluminum) is presented in a different column, and the flow direction is from top to bottom. Note that the viscosity decreases as the aluminum mass fraction increases from 45 to 55%; however, for the 60% aluminum the viscosity increases. This behavior is probably due to the change in the binding forces between the gel matrix and the aluminum particles. The phenomenon is rather complex, and further analysis is required. Although these results have a little quantitative significance, they indicate the existence of an optimal metal loading.

The effect of the convergence angle for the RP-1/Al gels is shown in Figs. 8a and 8b for the 45% aluminum mass fraction. The effect of the metal loading for a convergence angle of 5 deg is shown in Figs. 9a and 9b.

The flowfield was also solved for the three water gels type X with various gellant fractions, as shown in Fig. 10. In this case also, viscosity reduces significantly with axial distance. The effect becomes more dramatic as the gellant percentage increases. This is expectable because the fluid behavior becomes more Newtonian as the gellant fraction decreases.

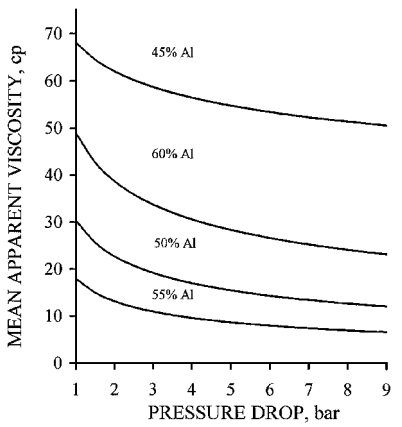

a) Mean apparent viscosity vs pressure drop

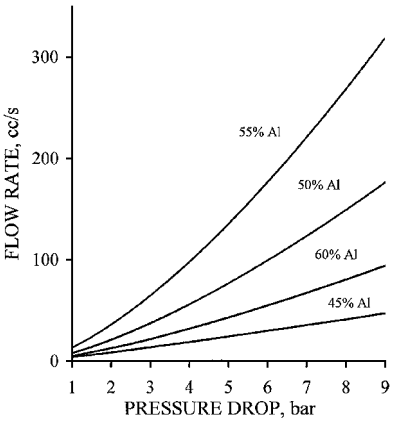

b) Flow rate (approximate within a 2% range for the preceding gels) vs pressure drop

Fig. 9 Metal loading effect, RP-1/Al gel with various aluminum mass fractions, L = 8 mm, R_L = 0.3 mm, α = 5 deg.

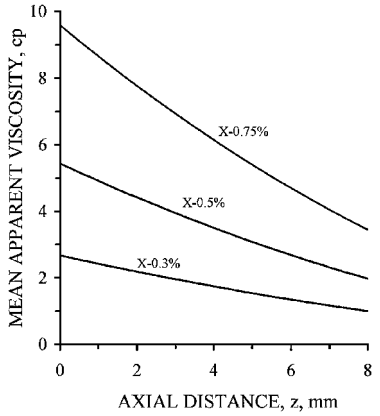

Fig. 10 Mean apparent viscosity along the axis for type X water gels, L = 8 mm, R_L = 0.4 mm, α = 2 deg, and ΔP = 2 bar.

Conclusions

The governing equations of the steady flow of gel propellants and fuels in a tapered tube injector have been formulated assuming a PL rheological model.

A parametric investigation was conducted to evaluate the effect of the injector geometry and pressure gradient on the flow rate and the mean apparent viscosity of the gel for various fuels and metal loadings.

The theoretical results indicate that the flow rate increases significantly with decreasing the PL index and with increasing the pressure drop in the injector. In the tapered injector, the apparent viscosity is not uniform in each cross section; it is maximal at the axis and reaches minimum at the wall.

The mean apparent viscosity of the gel exhibits a significant decrease with increasing the convergence angle of the injector. This implies that, to obtain better atomization of the gel, high convergence angles are required.

A comparison between RP-1/Al gels with various aluminum mass fractions was conducted. The results indicate the existence of an optimal metal loading.

Water gels exhibit the same flow behavior, and the effect becomes more significant as the gellant percentage increases.

References

[1]Schindler, R. C., Olson, A. M., and Arnold, C. J., "A Gelled Propellant Sustainer Stage," AIAA Paper 92-1122, Feb. 1992.

[2]Mueller, D. C., and Turns, S. R., "Some Aspects of the Secondary Atomization of Aluminum/Hydrocarbon Slurry Propellants," *Journal of Propulsion and Power*, Vol. 9, No. 3, 1993, pp. 345–352.

[3]Green, M. J., Rapp, D. C., and Roncace, J., "Flow Visualization of a Rocket Injector Spray Using Gelled Propellant Simulants," AIAA Paper 91-2198, June 1991.

[4]Guglielmi, J. D., "Atomization of JP-10 /B_4C Gelled Slurry Fuel," M.Sc. Thesis, Dept. of Aeronautics and Astronautics, Naval Postgraduate School, Monterey, CA, June 1992.

[5]Rapp, D. C., and Zurawski, R. L., "Characterization of Aluminum/RP-1 Gel Propellant Properties," AIAA Paper 88-2821, July 1988; also NASA TM-100951, Oct. 1988.

[6]Palaszewski, B., and Powell, R., "Launch Vehicle Performance Using Metallized Propellants," AIAA Paper 91-2050, June 1991.

[7]Starkovich, J., and Palaszewski, B., "Technology for Gelled Liquid Cryorenic Propellants: Metallized Hydrogen/Aluminum," AIAA Paper 93-1878, June 1993.

[8]Bird, R. B., Armstrong, R. C., and Hassager, O., *Dynamics of Polymeric Liquids*, Wiley, New York, 1977, pp. 169–253.

[9]Yarin, A. L., "*Free Liquid Jets and Films: Hydrodynamics and Rheology*," Longman House, England and John Wiley & Sons, Inc., New York, 1993, pp. 349–396.

[10]Gupta, B. L., Varma, M., and Munjal, N. L., "Rheological Studies on Virgin and Metallized Unsymmetrical Dimethyl Hydrazine," *Propellants, Explosives, Pyrotechnics*, Vol. 11, No. 1, 1986, pp. 45–52.

[11]Zeigier, E. H., and Stanley, N. F., "Shock Gel Process for Small Arms Gun Propellant," Rept. prepared for Dept. of the Army, DAAA25-73-C0172, Hercules Inc., Allegany Ballistics Lab., Cumberland, MD, June 1976.

[12]Muller, F. L., and Davidson, J. F., "Rheology of Shear Thinning Polymer Solutions," *Industrial and Engineering Chemistry Research*, Vol. 33, No. 10, 1994, pp. 2364–2367.

[13]Vinogradov, G. V., and Malkin, A. Y., *Rheology of Polymers, Viscoelasticity and Flow of Polymers*, Mir, Moscow, 1980, pp. 102–215.

[14]Skelland, A. H. P., *Non-Newtonian Flow and Heat Transfer*, Wiley, New York, 1967, pp. 68–156.

[15]Kozicki, W., and Tiu, C., "Parametric Modeling of Flow Geometries in Non-Newtonian Flows," *Rheology and Non-Newtonian Flows*, Vol. 7, *Encyclopedia of Fluid Mechanics*, Gulf Publ. Co., Houston, 1986, pp. 199–252.

[16]Cheremisinoff, N. P., "Rheological Characterization and Processability Testing," *Rheology and Non-Newtonian Flows*, Vol. 7, *Encyclopedia of Fluid Mechanics*, Gulf Publ. Co., Houston, 1986, pp. 991–1060.

[17]Ta-Jo, L., "Fully Developed Flow of Power-Law Fluids in Ducts," *Industrial and Engineering Chemistry Fundamentals*, Vol. 22, No. 1, 1983, pp. 183–186.

[18]Karagiannis, A., Mavridis, H., Hrymak, A. N., and Vlachopoulos, J., "A Finite Element Convergence Study for Shear-Thinning Flow Problems," *International Journal for Numerical Methods in Fluids*, Vol. 8, No. 2, 1988, pp. 123–138.

[19]Syoten, O., and Tadayoshi, M., "Theory of the Steady Slow Motion of Non-Newtonian Fluids Through a Tapered Tube," *Japanese Journal of Applied Physics*, Vol. 8, No. 1, 1969, pp. 5–8.

[20]Sutterby, J. L., "Laminar Converging Flow of Dilute Polymer Solutions in Conical Sections, II," *Transactions of the Society of Rheology*, Vol. 9, No. 2, 1965, pp. 227–241.

[21]Syoten, O., "Pressure Development in a Non-Newtonian Flow Through a Tapered Tube," *Biorheology*, Vol. 10, No. 2, 1973, pp. 207–212.

[22]Papanastasiou, T. C., *Applied Fluid Mechanics*, Prentice–Hall, Upper Saddle River, NJ, 1994, pp. 443–447.

[23]Dijksman, J. F., and Savenije, E. P. W., "The Flow of Non-Newtonian Liquids Through Annular Converging Regions," *Rheologica Acta*, Vol. 24, No. 2, 1985, pp. 105–118.

[24]Chojnacki, K. T., and Feikema, D. A., "Atomization Studies of Gelled Bipropellant Simulants Using Planar Laser-Induced Fluorescence," AIAA Paper 95-2423, July 1995.